Prolidase is required for early trafficking events during influenza a virus entry

Pohl, M O ; Edinger, T O ; Stertz, S

Abstract: Influenza A virus (IAV) entry is a multistep process that requires the interaction of the virus with numerous host factors. In this study, we demonstrate that prolidase (PEPD) is a cellular factor required by IAV for successful entry into target cells. PEPD was selected as a candidate during an entry screen performed on nonvalidated primary hits from previously published genome-wide small interfering RNA (siRNA) screens. siRNA-mediated depletion of PEPD resulted in the decreased growth of IAV during mono- and multicycle growth. This growth defect was independent of cell type or virus strain. Furthermore, IAV restriction was apparent as early as 3 h postinfection, and experiments in the absence of protein biosynthesis revealed that the nuclear import of viral ribonucleoprotein complexes (vRNPs) was already blocked in the absence of PEPD. These results led us to investigate which step during entry was affected. Receptor expression, IAV attachment, or IAV internalization was not dependent on the presence of PEPD. However, when looking at the distribution of incoming IAV particles in PEPD-knockdown cells, we found a localization pattern that differed from that in control cells: IAV mostly localized to the cell periphery, and consequently, viral particles displayed reduced colocalization with early and late endosome markers and fusion between viral and endosomal membranes was strongly reduced. Finally, experiments using a competitive inhibitor of PEPD catalytic activity suggested that the enzymatic function of the dipeptidase is required for its proviral effect on IAV entry. In sum, this study establishes PEPD as a novel entry factor required for early endosomal trafficking of IAV. IMPORTANCE: Influenza A virus (IAV) continues to be a constant threat to public health. As IAV relies on its host cell for replication, the identification of host factors required by the virus is of importance. First, such studies often reveal novel functions of cellular factors and can extend our knowledge of cellular processes. Second, we can further our understanding of processes that are required for the entry of IAV into target cells. Third, the identification of host factors that contribute to IAV entry will increase the number of potential targets for the development of novel antiviral drugs that are of urgent need. Our study identifies prolidase (PEPD) to be a novel entry factor required by IAV for correct routing within the endosomal compartment following virus internalization. Thereby, we link PEPD, which has been shown to play a role during collagen recycling and growth factor signaling, to early events of viral infection.

DOI: https://doi.org/10.1128/JVI.00800-14

Pohl, M O; Edinger, T O; Stertz, S (2014). Prolidase is required for early trafficking events during influenza a virus entry. Journal of Virology, 88(19):11271-11283.
DOI: https://doi.org/10.1128/JVI.00800-14

Prolidase (PEPD) is required for early trafficking events during influenza A virus entry

Running title: Role of PEPD as influenza A virus entry factor

Marie O. Pohl[1; 2], Thomas O. Edinger[1; 2] and Silke Stertz[1*]

[1] Institute of Medical Virology, University of Zurich, 8057 Zurich, Switzerland,

[2] Life Sciences Zurich Graduate School, ETH and University of Zürich, 8057 Zurich, Switzerland

* corresponding author: Silke Stertz, Ph.D.

e-mail: stertz.silke@virology.uzh.ch

phone: +41 44 634 2899

fax: +41 44 634 4967

Abstract

Influenza A virus (IAV) entry is a multi-step process that requires the interaction of the virus with numerous host factors. In this study, we demonstrate that prolidase (PEPD) is a cellular factor required by IAV for successful entry into target cells. PEPD was selected as a candidate during an entry screen performed on non-validated primary hits from previously published genome-wide siRNA screens. siRNA-mediated depletion of PEPD resulted in decreased growth of IAV during mono- and multi-cycle growth. This growth defect was independent of cell type or virus strain. Furthermore, IAV restriction was apparent as early as 3h post-infection and experiments in the absence of protein biosynthesis revealed that nuclear import of viral ribonucleoprotein complexes (vRNPs) was already blocked in the absence of PEPD. These results led us to investigate which step during entry was affected. Receptor expression, IAV attachment or internalization were not dependent on the presence of PEPD. However, when looking at the distribution of incoming IAV particles in PEPD knockdown cells, we found a localization pattern that differed compared to control cells: IAV mostly localized to the cell periphery and consequently, viral particles displayed reduced co-localization with early and late endosome markers and fusion between viral and endosomal membranes was strongly reduced. Finally, experiments using a competitive inhibitor of PEPD catalytic activity suggest that the enzymatic function of the dipeptidase is required for its proviral effect on IAV entry. In sum, this study establishes PEPD as a novel entry factor required for early endosomal trafficking of IAV.

Importance

Influenza A virus (IAV) continues to be a constant threat to public health. As IAV relies on its host cell for replication the identification of host factors required by the virus is of importance: First, such studies often reveal novel functions of cellular factors and can extend our knowledge of cellular processes. Second, we can further our understanding of processes that are required for entry of IAV into target cells. Third, the identification of host factors that contribute to IAV entry will enlarge the number of potential targets for the development of novel antiviral drugs that are of urgent need. Our study identifies prolidase (PEPD) as a novel entry factor of IAV required for correct routing within the endosomal compartment following virus internalization. Thereby, we link PEPD which has been shown to play a role during collagen recycling and growth factor signaling, to early events of viral infection.

Introduction

Influenza A virus (IAV), causes an acute febrile illness in humans generally referred to as the flu. The virus is responsible for causing annual epidemics and occasional pandemics which pose a threat to public health and a large economic burden on society. IAV belongs to the family of *Orthomyxoviridae* and contains a segmented, single-stranded RNA genome of negative polarity (1). IAV virions are enveloped and four membrane-associated proteins have been described: Hemagglutinin (HA), Neuraminidase (NA), the Matrix protein 2 (M2) ion channel (1) and the M2-related protein M42 (2). While NA is required for budding and release of viral progeny from infected cells, HA and M2 mediate entry of IAV virions into target cells which are thought to be primarily epithelial cells of the respiratory tract expressing sialic acid (3). Entry of IAV is a dynamic multi-step process that can be divided into several distinctive stages: attachment to the cell surface, internalization, endosomal transport of virions towards the perinuclear region, fusion, uncoating and import of the viral ribonucleoprotein complexes (vRNPs) into the nucleus (4). The receptor for IAV attachment is sialic acid (1). HA binds to sialic acid residues present on many cell-surface glycoproteins which triggers uptake of virions into target cells. Internalization occurs mainly via clathrin-mediated endocytosis (5-7) but also alternative pathways such as macropinocytosis have been proposed (8, 9). The pH-drop that occurs during the maturation process from early endosomes (EE) to late endosomes (LE) is required for a conformational change of HA which mediates fusion of viral and endosomal membranes (10-12). Simultaneously, the M2 ion channel allows flux

77 of protons from the endosomal compartment into the virion core (13). The
78 resulting acidification of the virion is required for release of the vRNPs into the
79 cytoplasm, a process referred to as uncoating (14). Finally, vRNPs are imported
80 into the nucleus, the site of viral replication, via the karyopherin transport
81 pathway (1, 15).

82 Vaccines against IAV are available and are the best option at present to prevent
83 seasonal epidemics. However, these vaccines induce only short-lived protection
84 against a small set of viruses. They do not provide protection against new strains
85 of IAV that occasionally arise in the human population. For such a scenario it is
86 crucial to have anti-influenza virus drugs available. Currently, there are two
87 different classes of antiviral drugs approved for the use in humans. One class are
88 the adamantanes which target the M2 ion channel thereby preventing uncoating
89 (16-18). The second class of drugs targets NA and inhibits egress of the virus
90 from the host cell (19, 20). Unfortunately, resistance of IAV against these drugs
91 has become a major problem such that the adamantanes are not recommended
92 for the use in humans anymore (21). In addition, virus strains resistant against
93 NA inhibitors have been reported (22). These developments emphasize the
94 urgent need for novel antiviral treatment options. To circumvent the problem of
95 resistance and to increase the number of potential targets of novel antivirals,
96 several studies are currently directed towards finding cellular proteins instead of
97 viral proteins as drug targets. Genome-wide siRNA screens are a powerful tool to
98 identify host factors associated with viral infections. Several such screens have
99 been performed to determine cellular factors required by IAV during infection (23-

30). Surprisingly, there was hardly any overlap between the primary hits identified in these screens (31). Responsible for these discrepancies are likely the different experimental designs as well as the selection criteria and validation methodologies applied in the screens. This complicates the comparison between hits from different screens and may account for the small overlap observed. For follow-up studies, the factors that show up in several screens are thus far the best candidates. In this study, we aimed to revisit the overlapping primary hits from the different screens that had not been validated yet and screen them for a role during IAV entry. We identified PEPD, a cytosolic dipeptidase, as a novel entry factor of IAV and show that the distribution of incoming viruses was altered in cells lacking PEPD and that there were fewer viruses present in the endosomal compartment. These data indicate that the routing of IAV following internalization is likely to be dependent on PEPD. Finally, we show that the catalytic activity of PEPD may be required for the observed pro-viral effect of PEPD on IAV entry.

Materials and Methods

Cells, viruses, and compounds. A549, MDCK and WI38 cell lines were maintained in 10% FCS-supplemented DMEM containing penicillin/streptomycin (Life Technologies). Influenza virus strain A/WSN/33 was grown in A549 cells, while A/Hong Kong/68, FPV/Dobson and A/Panama/2007/99 were grown in embryonated chicken eggs. A/Netherlands/602/2009 was grown in MDCK cells. Purified A/PR/8/34 was purchased from Charles River. All influenza virus stocks were titered by plaque assay using Vero or MDCK cells. Virus-like particles (VLP) were generated by transfecting 293T cells with a plasmid containing an HIV provirus encoding *Gaussia* luciferase, an HIV gag-pol expression plasmid and plasmids coding for the respective viral glycoproteins (WSN-HA/NA, LASV-GP or MLV-Env) using jetPRIME (Polyplus transfection) (28). The following compounds were used: Bafilomycin A1 (Sigma-Aldrich), N-Benzyloxycarbonyl-L-proline (Chemos GmbH), cycloheximide (Sigma-Aldrich), recombinant PEPD (Abnova) and IFN-alfa 2a from Roche (Roferon-A).

siRNA transfections and cell viability assay. Cells were transfected in suspension with 30 nM siRNA (Qiagen) diluted in Opti-MEM (Life Technologies) using RNAimax (Invitrogen). 48h post-transfection cells were either infected or cell viability was determined using CellTiter-Glo (Promega). For siRNA and DNA co-transfection, A549 cells were transfected with 30nM siRNA and 200ng of plasmid DNA diluted in Opti-MEM using Lipofectamine 2000 reagent (Life Technologies).

Entry screen and virus-like particle infection. Per factor, four siRNAs (Qiagen, see suppl. Table 1) were used for transfection into A549 cells. Only two siRNAs per gene were used if siRNAs were functionally verified by Qiagen. 48h post-transfection, cells were infected with VLPs diluted in Opti-MEM for 1h at 37ºC. Cells were washed with phosphate-buffered saline (PBS) and then kept in DMEM supplemented with 10% FCS and penicillin/streptomycin for 30h at 37ºC. Luciferase activity in the supernatants was determined using the Renilla Luciferase Assay System (Promega). siRNAs that induced reductions in cell viability of more than 30% compared to siScr treatment were excluded from the analysis. The quality of reduction in IAV VLP entry was scored based on the fulfillment of the following criteria: A reduction in IAV VLP entry of more than 50% compared to control, while LASV or MLV VLP entry was higher than 50% scored 1. To score 2, luciferase counts had to be below 30% compared to control for IAV VLPs while the reduction for either LASV or MLV VLPs was less than 70%. Finally, the highest score of 3 was given if siRNA-transfection resulted in reductions of IAV VLP entry of more than 70% of the control values while LASV or MLV VLP entry was not reduced more than 50% compared to siScr-treated cells. A gene was considered an entry factor if at least 2 siRNAs fulfilled one of the three criteria. With these criteria we aimed to find IAV-specific host factors. We included scoring of control VLPs (LASV and MLV) because effects on the luciferase activity following infection with these VLPs would indicate either general effects on viral entry mechanisms or effects on the retroviral steps during this assay. Next, the sum of all scores obtained for a given factor was calculated.

This was then multiplied with the ratio (R) of the number of successful siRNAs to the total number of siRNAs tested for a given factor.

Influenza A virus infection. A549 or WI38 cells were washed once with PBS, then infected with the respective amount of virus diluted in PBS supplemented with 0.02 mM Mg^{2+}, 0.01 mM Ca^{2+}, 0.3% bovine serum albumin (BSA) and 1% penicillin/streptomycin (infection PBS) at 37°C for 1h before changing to DMEM containing 0.3% BSA, 20 mM HEPES and 1% penicillin/streptomycin (post-infection DMEM). With the exception of A/WSN/33 all virus strains were grown in the presence of 0.25 ug/ml TPCK trypsin (Sigma-Aldrich). Virus titers in tissue culture supernatants were determined by standard plaque assay on Vero or MDCK cells.

Western blotting. Cell extracts were prepared using Laemmli buffer (62.5 mM Tris-HCl pH 6.8, 25% glycerol, 2% SDS, 350mM DTT, 0.01% Bromophenol Blue). Samples were subjected to standard SDS-PAGE and proteins were transferred to nitrocellulose membranes (Hybond ECL, GE Healthcare). For blocking, 5% milk diluted in Tris-buffered saline containing 0.5% Tween 20 was used. The following primary antibodies were used: rabbit monoclonal anti-PEPD (Abcam, ab86507); mouse monoclonal anti-MxA (kind gift of J. Pavlovic); mouse monoclonal anti-β-actin (Santa Cruz Biotechnology, sc-47778); rabbit polyclonal anti-NP (kind gift of A. Nieto); mouse monoclonal anti-M1 (kind gift of J. Pavlovic).

Immunofluorescence. To synchronize infection, A549 cells were infected with A/WSN/33 on ice for 1h. Then, cells were shifted to 37ºC for the indicated times to allow infection to proceed. For NP staining, cells were fixed with 3.7% paraformaldehyde (PFA) in PBS, permeabilized with 0.5% Triton-X-100 and blocked with 2% bovine albumine. Cells were incubated with mouse monoclonal anti-NP (kind gift of J. Pavlovic). The NP/EEA1 or LBPA co-staining was performed in PBS supplemented with 50 mM NH_4Cl, 0.1% saponin and 2% bovine albumine (confocal buffer). The following primary antibodies diluted in confocal buffer were used: rabbit monoclonal anti-NP (kind gift of P. Palese); mouse monoclonal anti-EEA1 (BD Biosciences) and mouse monoclonal anti-LBPA (Echelon), followed by secondary antibodies (Life Technologies, A-21121, A-21134 and A-11008). Nuclei were visualized using DAPI (Life Technologies) or DAPI Fluoromount G (Southern Biotech #0100-20). For labeling acidic organelles a Lysotracker system was used (Life Technologies Lysotracker Red DND-99, L7528). Images were acquired with a Leica SP5 confocal laser-scanning microscope. Image processing was performed using LAS AF lite Software (Leica), Imaris (co-localization and z-stack analysis) and ImageJ (nuclear signal intensity analysis and fusion site analysis). A Mann-Whitney test was used to test for significant differences in mean nuclear fluorescence intensity.

Internalization assay and FACS. A/WSN/33 was concentrated over a sucrose cushion (30%) and biotinylated using the EZ-link NHS-SS Biotin kit (Thermo Scientific). siRNA-transfected A549 cells were detached (EDTA-Trypsin, Life Technologies) and cooled down in FACS buffer (PBS supplemented with 2%

BSA) on ice. Cells were infected on ice with biotinylated A/WSN/33 for 1h and washed thoroughly with FACS buffer. Before cells were incubated at 37ºC for 30 minutes, cells were incubated on ice either with FACS buffer containing unconjugated streptavidin (2 mg/ml, Life Technologies) or FACS buffer alone. Following internalization, cells were either directly fixed with PFA (3%) or incubated with FACS buffer supplemented with streptavidin and sodium azide 0.1% for 30 minutes and then fixed. For permeabilization Triton X-100 0.5% diluted in PBS was used. For staining, Cy3-labeled streptavidin (Life Technologies) diluted in FACS buffer was used. Sialic acid was stained using *Sambucus nigra* and *Maackia amurensis* lectins (Reactolab SA). FACS analysis was performed on a CyAn ADP Analyzer (Beckmann Coulter Inc.) and data were analyzed using FlowJo software.

Fusion Assay. Measurement of viral fusion was performed according to the protocol previously described in (32). In brief, IAV A/PR/8/34 was labeled using two fluorescent dyes, R18 and SP-DiOC18 (Molecular Probes), in a ratio 1:2 with final concentrations of R18=22 µM and SP-DiOC18=46 µM. After intense vortexing for 1 hour labeled virus was filtered through a 0.22 µm pore filter. Virus was cold-bound to the cells for 30 min and after washing with PBS temperature was shifted to 37 °C for either 0, 90 or 180 minutes. Unfixed and unpermeabilized samples were mounted with DAPI Fluoromount G and images were acquired on a Leica SP5 confocal laser scanning mircroscope. Image analysis was carried out using the spot analysis function of Image J for SP-

DiOC18 staining with a distinct spot size of 20 pixels and a subsequent correction for cell numbers.

Results

PEPD was identified as a potential entry factor during a virus-like particle based entry screen.

The above described genome-wide siRNA screens identified numerous factors to be involved in IAV infection. To uncover potential entry factors of IAV, we decided to revisit the primary hits of four published siRNA screens (24-26, 28) that lacked experimental validation and screen them for a role during the IAV entry process. We included only those factors that were identified during at least two (or more) out of the four published screens in order to increase the confidence of finding an association with IAV infection. As we were primarily interested in virus entry we excluded factors with a known nuclear function such as splicing factors (Fig 1A). The remaining 43 factors were screened for a role during IAV entry using a virus-like particle (VLP)-based entry assay: We used VLPs that carry IAV glycoproteins on their surface and contain a reporter gene for convenient readout. These VLPs mimic IAV particles but carry a *Gaussia* luciferase reporter gene. Human lung A549 cells were transfected with siRNAs to achieve knockdown of the respective candidate genes. Per factor, four different siRNAs were used to exclude off-target effects. 48 hours post-transfection, cells were infected with VLPs and luciferase counts were measured 30 hours post-infection as an indicator of entry efficiency. To counterscreen for non-entry related effects, VLPs carrying the envelopes of Lassa virus (LASV) or Murine

253 Leukemia virus (MLV) were included. LASV also enters target cells by
254 endocytosis but bypasses early steps of endosomal trafficking (33). In contrast,
255 MLV is known to enter target cells via membrane fusion (34). Entry factors were
256 defined as genes that, upon knockdown with at least two siRNAs, resulted in
257 inhibition of IAV-VLP entry but not of VLPs carrying glycoproteins of LASV or
258 MLV. In total, 22 factors were shown to be associated with IAV entry (Fig 1A and
259 B). We calculated an entry score that is based on the number of siRNAs per
260 gene that induced IAV-specific reduction of VLP entry and the degree of
261 reduction compared to controls. The entry score was subsequently used to rank
262 the identified entry factors (Fig 1B). siRNAs targeting subunits of the endosomal
263 vATPase reduced IAV VLP entry most strongly (Fig 1B and C). The vATPase
264 mediates the acidification of endosomes and is known to be required for efficient
265 entry of IAV (35, 36) thereby acting as internal control for our entry screen.
266 Another well-perfoming candidate was prolidase (PEPD), a ubiquitously
267 expressed cytosolic peptidase that cleaves dipeptides with a proline or
268 hydroxyproline at the C-terminus. Three out of four PEPD-specific siRNAs
269 potently reduced IAV VLP entry but not control VLPs (Fig 1C and Suppl. Table
270 1). Besides its dipeptidase function, PEPD has been shown to be involved in
271 epidermal growth factor recetor (EGFR) family signalling (37, 38). EGFR
272 signalling is believed to play a role during IAV infections (39, 40). In addition,
273 gene ontology analysis of the validated hits of the siRNA screens revealed
274 kinase signalling as the most overrepresented category (31). Therefore, we
275 chose PEPD as a candidate for follow-up studies. Efficient knockdown of

endogenous as well as overexpressed PEPD protein levels were confirmed by western blot (Fig 1D). Moreover, cell viability 48h after siRNA transfection was assessed to exclude false-positive effects due to increased cell death (Fig 1E). To exclude that siRNA transfection alone stimulated interferon (IFN) production, thereby reducing VLP entry in PEPD knockdown cells due to expression of antiviral genes, we detected protein levels of MxA, an IFN-inducible gene, in A549 cells 48h after siRNA transfection. No MxA induction was observed in siPEPD or siScr transfected cells. Only following stimulation with IFN, MxA was detectable (Fig 1F). These data suggest that PEPD is required during the IAV entry process and we therefore selected PEPD as a candidate for follow-up studies on IAV entry.

PEPD is required for growth of IAV.

Next, we investigated whether knockdown of PEPD also affected growth of wild-type IAV. We transfected A549 cells with siRNAs targeting PEPD or with a control siRNA. Cells were infected with A/WSN/33 with a low MOI (0.01) to allow multi-cycle growth. 24 hours post-infection, tissue culture supernatants were harvested and viral titers were determined by plaque assay. Depletion of PEPD reduced viral titers strongly compared to siScr transfected cells (Fig 2A). Similar growth defects of A/WSN/33 were observed in WI38 cells, a primary lung fibroblast cell line (Fig 2B). In addition, IAV strains FPV/Dobson (H7N7), A/Hong Kong/68 (H3N2), A/Netherlands/602/2009 (H1N1) and A/Panama/2007/99 (H3N2) also displayed reduced growth in A549 cells upon PEPD knockdown (Fig

298 2C-F), indicating that the observed phenotype is virus strain and cell line
299 independent.

300 **Depletion of PEPD affects an early step during the IAV life cycle.**

301 To determine whether IAV growth is also affected during mono-cycle growth, we
302 monitored viral protein production 6h post infection in siRNA-treated A549 cells.
303 Knockdown of PEPD resulted in decreased protein levels of M1 in western blot
304 analysis (Fig 3A). Next, siRNA transfected A549 cells were infected with
305 A/WSN/33 with a high MOI (10) for 3h and viral NP protein expression was
306 visualized by confocal microscopy. In siScr treated cells, a strong NP signal was
307 detected in the nuclei of infected cells (Fig 3B) while in cells depleted of vATPase
308 barely any nuclear NP was detectable. Following transfection of siRNAs targeting
309 PEPD, nuclear NP expression was largely absent, similar to vATPase
310 knockdown cells. The magnitude of NP-signal reduction was dependent of the
311 siRNA used (Fig 3C). Transfection of siPEPD_1 inhibited the virus to a greater
312 extent than siPEPD_2 and these data are consistent with the viral titers (Fig 2)
313 and M1 expression levels (Fig 3A) measured before. In the presence of
314 cycloheximide, when *de novo* synthesis of NP is blocked due to inhibition of
315 protein biosynthesis, nuclear NP signal intensity was still lower in siPEPD_1 cells
316 compared to control cells (Fig 3D). These data suggest that nuclear import of
317 vRNPs is already impaired in the absence of PEPD.

318 **Knockdown of PEPD reduces fusion events during IAV infection.**

We next aimed to investigate whether the reduction of nuclear NP in PEPD knockdown cells was due to a defect in virus entry or due to a block during later events such as uncoating or transport of vRNPs into the nucleus. Therefore, we generated a dually fluorescent virus, labeled with SP-DiOC18 and R18 that allows the detection of fusion events. Both dyes are lipophilic and are inserted into the viral envelope upon labeling. This virus appears red fluorescent as the R18 dye (red) quenches the SP-DiOC18 dye (green) within the envelope of the virion (32). At the end of the viral entry process however, when viral and endosomal membranes merge, both dyes disperse within the endosomal membranes and the green fluorescent signal increases due to dequenching. To measure whether fusion is taking place in the absence of PEPD, we infected A549 cells 48h after siRNA transfection on ice with R18/SP-DiOC18-labelled A/PR/8/34. Then, cells were shifted to 37°C for 0, 90 or 180 minutes to allow entry and fusion of the labeled viruses. During the experiment, either DMSO 0.1% or 10 nM bafilomycin A1 was present in the medium. Bafilomycin A1 is an inhibitor of vATPases and prevents acidification of endosomes and thus blocks IAV fusion (41). In control cells, large green fluorescent fusion sites were detectable after 90 and 180 minutes but not after 0 minutes of infection (Fig 4 A and B). Cells depleted of vATPase had a reduced number of fusion sites compared to siScr-treated cells. Also in siPEPD-transfected cells, significantly less fusion sites were counted following both, 90 minutes and 180 minutes of infection (Fig 4A and B). Treatment with bafilomycin A1 potently inhibited viral fusion in all cells tested (Fig 4C). These data strongly suggest that indeed, PEPD

342 plays a role during the IAV entry process as fusion is impaired to comparable
343 levels to vATPase depleted cells. Thus, PEPD is required by the virus for efficient
344 fusion or earlier during entry.

345 **PEPD is not required for attachment or internalization of IAV.**

346 We continued to identify the step affected during IAV entry in the absence of
347 PEPD. The first step of the entry process is the attachment of the virus to the
348 host cell membrane. To assess whether PEPD is required for receptor
349 expression we measured the amount of both, α2'-3' and α2'-6' linked sialic acid
350 expressed on the surface of A549 cells 48 hours after siRNA transfection. As
351 depicted in Figure 5A, there was no difference in the amount of both types of
352 receptors on PEPD knockdown cells compared to control cells as measured by
353 FACS. We next investigated the effect of PEPD depletion on IAV attachment and
354 internalization. Therefore, we generated biotinylated A/WSN/33 that can be
355 visualized through staining with fluorescently labeled streptavidin. siPEPD or
356 siScr transfected A549 cells were incubated on ice with this biotinylated virus,
357 allowing only attachment of virions to the cell membrane but preventing
358 internalization. Cell-bound virus was detected using cy3-labeled streptavidin.
359 This signal was completely abrogated when cells were incubated with unlabeled
360 streptavidin before fixation and subsequent staining (Fig 5B). There was no
361 difference detectable in the amount of virus attached to cells treated with siRNAs
362 targeting PEPD or control siRNAs. In order to measure internalized particles,
363 virus-attached cells were incubated at 37ºC for 30 minutes. Following incubation,
364 cells were either treated with unlabeled streptavidin or PBS before fixation,

365 permeabilization and staining with cy3-labelled streptavidin. External application
366 of unlabeled streptavidin could only partially reduce the virus-derived signal
367 indicating that most of the virions were taken up into the cells (Fig 5B). The
368 relative amount of internalized virus was calculated as the ratio of virus detected
369 after 30 minutes following unlabeled streptavidin incubation to virus detected
370 after 30 minutes washed only with PBS (Fig 5C). Notably, similar amounts of
371 virus were internalized in siPEPD-treated cells in comparison to control cells. To
372 confirm that virus uptake was not affected in the absence of PEPD we visualized
373 SP-DiOC18-labeled A/WSN/33 after 30 minutes of infection. Z-stack images
374 clearly revealed virus inside cells depleted of PEPD (Fig 5D). Taken together, we
375 were able to demonstrate that siRNA-mediated knockdown of PEPD does neither
376 influence IAV attachment to target cells nor virus internalization.

377 **Incoming virus exhibits a different localization pattern in PEPD depleted**
378 **cells.**

379 Our data so far suggest that IAV requires PEPD during the entry process after
380 internalization and before or during fusion. Next, we investigated trafficking of
381 incoming virus particles in siRNA-treated cells deficient of PEPD. Cells were
382 infected with A/WSN/33 with MOI of 25 and virus was visualized after 0, 30, 60,
383 90, and 180 minutes through staining of NP which is very abundant in IAV virions
384 (42). In control cells, IAV was detectable in the cytoplasm of infected cells at
385 early time points (30 and 60 minutes post-infection) while after 90 and 180
386 minutes of infection, NP was also detectable in the cell nuclei (Fig 6A). The
387 strong signal 180 post infection was largely due to *de novo* synthesis and could

388 be abrogated through treatment with cycloheximide (data not shown).
389 Nevertheless, similar to the data presented in Figure 3D, NP was present in the
390 nuclei of cells in the presence of the drug, indicating that nuclear import of
391 vRNPs was effective in siScr-transfected cells. Following PEPD knockdown
392 however, the distribution of PEPD was largely different to control cells: The NP
393 signal appeared predominantly in the cell periphery during all time points
394 measured (Fig 6A). Even after 180 minutes, only few nuclei showed *de novo* NP
395 synthesis, this is in correspondence to the data presented in Figure 3B. Instead,
396 most of the signal was visible in proximity to the plasma-membrane of the cells.
397 This distinctive localization pattern of NP in siPEPD-transfected cells suggests
398 that early virus sorting and trafficking within the endosomal compartment may be
399 affected. The morphology and localization of early and late endosomes,
400 visualized through staining of the respective markers EEA1 and LBPA, was
401 indistinguishable in cells treated with siPEPD or siScr (Fig 6B). In addition,
402 staining of the endocytic machinery using lysotracker, a fluorescent dye that
403 labels acidic organelles, did not reveal differences between siPEPD and control
404 treated cells indicating that the endosomal compartment remains intact in the
405 absence of PEPD (Fig 6B). We next investigated the degree of co-localization of
406 incoming virions with early and late endosome markers in a time-course
407 experiment (Fig 6 C-E). In control cells, NP co-localized with the early endosome
408 marker EEA1 during early phases of infection (Fig 6D) and subsequently with the
409 late endosomal marker LBPA (Fig 6E). In cells transfected with siRNAs targeting
410 vATPase, a higher degree of co-localizaton was observed for NP and EEA1 at

411 early time points and with LBPA during late time points of infection (Fig 6D and
412 E). This is in line with a previous report showing that depletion of vATPase
413 results in accumulation of incoming viruses within endosomal compartments (43).
414 In contrast, at all time points measured, less NP co-localized with either EEA1 or
415 LBPA in PEPD deficient cells (Fig 6D and E). The retention of larger amounts of
416 virus in the cell periphery probably largely accounts for this observation. Taken
417 together, we demonstrate that in the absence of PEPD, incoming IAV
418 predominantly resides in the cell periphery leading to reduced association with
419 early and late endosomes as well as limited nuclear import and *de novo* NP
420 synthesis.

421 **Cbz-Pro, an inhibitor of the enzymatic activity of PEPD inhibits IAV at an**
422 **early step of the infection cycle.**

423 As PEPD possesses dipeptidase activity, we tested whether this catalytic activity
424 mediates the proviral effects of PEPD. To this aim, we used Cbz-Pro, a
425 competitive inhibitor of PEPD catalytic activity (44). In human fibroblasts it has
426 been shown that 10mM of Cbz-Pro inhibits PEPD enzymatic activity to about
427 80% (45). Therefore, we decided to use 5 and 10 mM Cbz-Pro for our
428 experiments. Following 2h of pre-incubation, A549 cells were infected on ice with
429 A/WSN/33, MOI=10 in the presence of the inhibitor or control treatment. Then,
430 cells were shifted to 37ºC for 3h with inhibitor present in the media. Nuclear NP
431 expression was monitored by confocal microscopy. Cbz-Pro reduced the amount
432 of nuclear NP compared to cells treated with the solvent methanol (Fig 7A).
433 Treatment with 5mM Cbz-Pro had a small but significant effect on nuclear NP-

synthesis, while the higher concentration strongly inhibited nuclear NP signal (Fig 7A), indicating a dose-dependency. The reduction in NP signal was not due to cytotoxic effects of the inhibitor as shown in a cell viability assay for 5h treatment with the inhibitor (Fig 7B). Moreover, in the presence of cycloheximide, Cbz-Pro also reduced nuclear NP signal intensity, indicating that the inhibitor acts before viral protein synthesis (Fig 7C). We next tested whether bafilomycin A1 treatment following incubation with Cbz-Pro could maintain the inhibition of virus infection. A549 cells were incubated with Cbz-Pro for 2h prior to infection with WSN. After infection, cells were incubated in Cbz-Pro-containing medium for 1h at 37°C. Then, cells were incubated either with Cbz-Pro, solvent or bafilomycin A1. 3h post infection, nuclear NP signal intensity was measured by confocal microscopy. As shown in figure 7D, switching from Cbz-Pro treatment to bafilomycin A1 1h after infection resulted in a similar degree of inhibition as treatment with Cbz-Pro for 3h. Switching from Cbz-Pro to solvent-containing medium in turn resulted in markedly increased signal intensity of nuclear NP. These data indicate that Cbz-Pro treatment indeed targets viral entry before fusion. Taken together, our data indicate that the catalytic activity of PEPD is required for efficient entry of the virus into target cells.

PEPD has been shown to act as a ligand for members of the EGF receptor family when present in the extracellular space (37, 38). Furthermore, activation of EGFR has been implicated in IAV internalization (39). Therefore, we tested whether extracellularly provided recombinant PEPD can rescue virus infection following siRNA-mediated knockdown of intracellular PEPD. 48h after

transfection of siScr or siPEPD_1, A549 cells were infected with IAV MOI=10 on ice and nuclear NP signal intensity was determined following incubation for 3h at 37°C. It has been shown that 2.7nM PEPD suffices to activate EGFR (37). We decided to use 50nM PEPD during our experiments. Recombinant PEPD or vehicle was added to the medium either 1h before infection, during infection or 1h post-infection and was maintained until the end of the experiment. As shown in figure 7E, extracellular PEPD was not able to restore nuclear NP levels in siPEPD_1 treated cells. Thus, the effect of depletion of intracellular PEPD on IAV infection is independent of possible extracellular effects of PEPD on virus entry.

Discussion

In this study, we identify PEPD as a novel entry factor of IAV. We have demonstrated that upon knockdown of PEPD, IAV fusion events and the degree of co-localization with endosomal markers are strongly reduced. Instead, incoming IAV is retained in proximity to the plasma membrane. This suggests that PEPD is required for early endosomal routing of IAV during entry.

PEPD is a metalloprotease (46, 47) that catalyzes a rate-limiting step in the collagen-recycling pathway (48). During the degradation of collagen, PEPD cleaves dipeptides containing a proline or hydroxyproline at the C-terminus, thereby releasing free proline into the cytoplasm (48, 49). Mutations that result in loss of enzymatic activity give rise to prolidase deficieny (PD), a rare autosomal recessive disease in humans. PD is a connective tissue disorder and comprises a variety of symptoms such as mental retardation, skin ulcerations and recurrent

480 respiratory infections (48, 50-52). PEPD overexpression induces the expression
481 of HIF-1α-related gene products (53) as well as reduced NF-κB expression (48)
482 thereby providing a link between PEPD and the regulation of immune responses
483 such as cytokine production. In line with this, PD appears to be associated with
484 systemic lupus erythematosus, an auto-immune disorder. Thus, the complexity of
485 the disorder and the apparent distortion of barrier as well as immune functions
486 during long-term alteration of PEPD expression and -function may explain the
487 increased susceptibility to infections. However, PEPD has also been
488 demonstrated to be involved in a number of signaling pathways that are activated
489 during early phases of IAV infection: PEPD activity has been shown to be
490 positively regulated through Integrin-β1 receptor signaling (54). Echistatin, a
491 dysintegrin and receptor antagonist of Integrin-β1 (55), reduced PEPD activity
492 and expression, as well as levels of phosphorylated MAPK1 and MAPK2 (56).
493 Conversely, thrombin, an integrin activator, induced the opposite effects (56).
494 Interestingly, MAPK1 was also shown to be activated during IAV infection in a
495 biphasic manner (57). The early phase phosphorylation was already apparent 5-
496 30 minutes post-infection indicating that MAPK1 signaling is involved during IAV
497 entry. In addition, inhibition of PEPD activity with Cbz-Pro was reported to
498 decrease phospho-AKT and phospho-mTOR levels, while incubation of cells with
499 the PEPD products proline and hydroxyproline reversed this effect (45). The
500 AKT/mTOR signaling cascade has also been shown to be activated early during
501 IAV infection (58), indicating that IAV activates pathways that are positively
502 regulated by PEPD.

503 Moreover, a recent study by Yang and colleagues suggests that PEPD can bind
504 and activate EGFR and induce downstream signaling events (37). EGFR is a
505 receptor tyrosine kinase (RTK) that is upstream of MAPK1 and has been
506 implicated in IAV infection. During a recently published RNAi screen for host
507 factors of IAV, EGFR was one of the best performing candidates (29). In addition,
508 Eierhoff and colleagues have demonstrated that EGFR is activated following IAV
509 attachment, which in turn promotes uptake of virions into cells (39), thereby
510 providing evidence for a role of EGFR during IAV entry. Notably, PEPD only
511 activated EGFR when present in the extracellular space, e.g. through release
512 from injured cells. Similar data were obtained for ErbB2, a member of the EGF
513 receptor family (38). Our data in contrast indicate that the enzymatic activity of
514 PEPD may play a role for its pro-viral effects during IAV entry and that a step
515 following internalization but before fusion is affected after PEPD depletion and
516 inhibition of its enzymatic activity. Furthermore, our experiments using
517 recombinant PEPD indicate that extracellularly provided PEPD cannot
518 compensate for the depletion of intracellular PEPD and fails to rescue IAV
519 replication in cells treated with siRNAs targeting PEPD. Thus, to what extent
520 EGFR and other family members are involved in the PEPD-dependent regulation
521 of IAV entry remains to be determined. Our data together with other published
522 studies provide a link between PEPD activity, early signaling events induced by
523 IAV and the successful completion of IAV entry. However, further experiments
524 are required to elucidate the relationship between these events and their
525 contribution during IAV entry.

Taken together, we were able to show that PEPD is required by IAV early in infection and that in the absence of PEPD early viral trafficking events are altered leading to reduced amounts of virus within early and late endosomes and fewer fusion events. While systemically, PEPD may be involved in maintaining the barrier function and immunity to infections; our data indicate that on the cellular level, PEPD is involved in orchestrating IAV routing during the entry process. Nevertheless, the precise role of PEPD during IAV entry remains elusive and the mechanism of the pro-viral role of PEPD during IAV entry will be the subject of further studies.

Acknowledgements

This work was supported by a grant from the Swiss National Science Foundation (31003A_135278) to SSt. MOP is the beneficiary of a doctoral grant from the AXA Research Fund. We thank A. Helenius and Y. Yamauchi (ETH Zurich, Switzerland) for providing the protocol for the fusion assay. We also thank S. Kunz (University Hospital Lausanne, Switzerland) for providing the LASV-G expression construct.

Figure legends

Figure 1. Identification of PEPD through a screen for host factors involved in IAV entry.

A Overview of the screening process. **B** Positive hits of the entry screen. The darker the colour and the higher the entry score, the better was the performance of a given factor during the entry screen. **C** vATPase and PEPD depletion reduces entry of IAV VLPs. A549 cells transfected with siRNAs targeting vATPase or PEPD were infected with VLPs carrying IAV, LASV or MLV glycoproteins on their surface and encoding a luciferase reporter gene. Luciferase activity was measured at 30h post infection and luciferase of cells transfected with siScr was set to 100%. Error bars indicate standard deviation of triplicates. **D** PEPD Knockdown control. A549 cells were either transfected with siRNAs targeting PEPD or siScr alone, or co-transfected with siRNAs and a PEPD expression plasmid. PEPD protein levels after 48h were determined by western blot. Arrow indicates endogenous PEPD. Shown is a representative image of three independent experiments. **E** Cytotoxicity of PEPD-specific siRNAs 48h post-transfection. Values are relative to cells transfected with siScr. Error bars indicate standard deviation of triplicates. **F** Knockdown of PEPD does not induce MxA expression. A549 cells were transfected with siPEPD_1 or siScr. As positive control, siScr-transfected control cells were stimulated with IFN-α (100 U/ml) for 16h. 48h post-transfection MxA expression was measured by western blot.

Figure 2. PEPD is required for growth of different IAV strains.

A A/WSN/33 growth in A549 cells is reduced upon PEPD depletion. A549 cells were transfected with siRNAs against PEPD, NP or siScr. 48h post-transfection cells were infected with A/WSN/33 MOI=0.01. 24h post-infection, supernatants were harvested and viral growth was determined by plaque assay.Shown is one of three independent experiments performed in triplicates. Error bars indicate standard deviation. **B** Growth of A/WSN/33 in siRNA-transfected WI38 cells. Protocol as in (A) but WI38 cells were used. Virus titers were measured in tissue culture supernatants 24h and 48h post-infection.Shown is one out of three independent experiments. Error bars indicate standard deviation of triplicates. **C-F** Growth of different IAV strains in A549 cells transfected with siScr, siPEPD_1 or sivATPase**.** 48h post-transfection, cells were infected with FPV/Dobson (H7N7) with MOI=0.01 (C), A/Hong Kong/68 (H3N2) with MOI=1 (D), A/Netherlands/602/2009 (H1N1) with MOI=1 (E) or A/Panama/2007/99 (H3N2) with MOI=1 (F). 24h later, supernatants were harvested and viral titers were determined by plaque assay. Shown is one out of three independent experiments performed in duplicates. Error bars indicate standard deviation.

Figure 3. Depletion of PEPD affects an early step of the IAV life cycle.

A Early M1 expression is reduced by PEPD knockdown. A549 cells were transfected with siRNAs targeting PEPD or siScr. 48h post-transfection, cells were infected with A/WSN/33 MOI=1. 6h after infection, cells were lyzed and M1 expression was determined by western blot. **B** Immunofluorescence pictures

589 showing reduced nuclear NP signal in PEPD knockdown cells. siRNA transfected
590 A549 were infected on ice with A/WSN/33 MOI=10 for 1h. Then, cells were
591 incubated at 37°C for additional 3h. Cells were stained for NP expression (green)
592 and nuclei (blue) and analyzed by confocal microscopy. Scale bars equal 25 µm.
593 Shown are representative pictures of three independent experiments performed
594 in duplicates. **C** Quantification of (B). Nuclear NP signal intensity of 100 nuclei
595 per condition was quantified using ImageJ software and analyzed using the
596 Mann-Whitney test. Error bars indicate standard deviation. **D** Quantification of
597 imported nuclear NP. Experimental set-up as in (B) but during the experiment,
598 cycloheximide (100ug/ml) was present in the media. 87 nuclei were counted per
599 condition and analyzed using the Mann-Whitney test. Error bars indicate
600 standard deviation.

601 **Figure 4. Knockdown of PEPD reduces fusion events during IAV infection.**
602 **A** Reduced fusion of SP-DiOC18/R18-labelled virus in PEPD-depleted cells.
603 A549 cells were transfected with siRNAs targeting PEPD, vATPase or with siScr.
604 48h post-transfection cells were first pre-incubated with 10 nM bafilomycin A1 or
605 0.1% DMSO and then infected on ice with SP-DiOC18/R18-labelled A/PR/8/34
606 for 1h. After incubation at 37°C for 0, 90 or 180 min cells were analyzed by
607 confocal microscopy. Shown are images representative of the 90 minutes time
608 point from the DMSO-treated samples. Scale bars equal 10 µm. **B and C**
609 Quantification of (A).The number of fusion sites per cell was quantified using
610 ImageJ software. Cells treated with DMSO are shown in (B). Cells treated with

bafilomycin A1 (10nM) are depicted in (C). (B) and (C) show a quantification of one out of three independent experiments. Error bars indicate standard deviation.

Figure 5. Effect of PEPD knockdown on sialic acid expression, IAV attachment and uptake.

A PEPD knockdown does not influence surface sialic acid expression. A549 cells were treated with siRNAs against PEPD or with siScr, stained with *Sambucus nigra* or *Maackia amurensis* lectins recognizing either α2'-3' or α2'-6' sialic acid and analyzed by FACS. Shown is one out of three independent experiments. Per condition, 10000 cells were analyzed. **B and C** Virus attachment and internalization are not affected by PEPD knockdown. A549 cells were transfected with siRNAs targeting PEPD or siScr and were infected 48h later on ice with biotinylated A/WSN/33 for 1h. Cells were either fixed following infection or, virus was allowed to internalize for 30 minutes at 37ºC. In half of the samples plasma membrane-attached virus was masked using unlabeled streptavidin before permeabilization (+ strep). The other half was PBS treated. Following permeabilization, cells were stained with Cy3-labelled streptavidin and analyzed by FACS (B). The relative amount of internalized virus was calculated as the ratio of virus-positive cells at ‚30 min + strep' to ‚30 min without strep' (C). Shown is one out of three independent experiments. Per condition, 10000 cells were analyzed. **D** Visualization of IAV internalization. SP-DiOC18-labelled IAV was allowed to cold-bind to siScr or siPEPD treated A549 cells. Then, temperature was shifted to 37°C. After 30 minutes, cells were fixed and α2'-6' linked sialic acid on the cell surface was stained using *Sambucus nigra* lectin. Images were

taken using confocal microscopy. Scale bars equal 10 µm. Arrows indicate DiOC18-labeled, internalized virus. Representative images are shown.

Figure 6. Incoming virus exhibits a different localization-pattern in PEPD knockdown cells.

A Immunofluorescence pictures showing NP distribution in PEPD-depleted and control cells. A549 cells were transfected with siScr or siPEPD_1. 48 hours post-transfection, cells were infected with A/WSN/33 with MOI=25. At the indicated time points, cells were fixed, stained for viral NP and analyzed by confocal microscopy. Scale bars equal 25 µm. Shown is one out of three independent experiments. **B** Effect of PEPD knockdown on the morphology of the endocytic machinery**.** siRNA-transfected A549 cells were either stained for EEA1or LBPA or incubated with lysotracker reagent. Scale bars equal 10 µm. Representative images of two independent experiments are shown. **C** Incoming viruses display less co-localization with endosomes in PEPD-depleted cells. Experimental set-up as in (A). Cells were co-stained against NP (green) and either EEA1 or LBPA (red)**.** Shown are representative images of virus-infected cells after 30 minutes (EEA1) or 60 minutes (LBPA). Scale bars equal 10 µm. **D and E** Co-localization quantification of the EEA1 (D) and LBPA (E) staining. Confocal images were analyzed for co-localization using Imaris software. The Mann-Whitney test was used to test for statistical significance (siScr vs. siPEPD_1). Shown is one out of three independent experiments. Error bars indicate standard deviation.

Figure 7. Inhibition of PEPD enzymatic function restricts IAV early in infection.

A Nuclear NP expression in Cbz-Pro-treated cells. A549 cells were pre-treated for 2h with indicated amounts of Cbz-Pro or the solvent 0.5% MetOH. Cells were infected on ice with A/WSN/33 MOI=10 and afterwards shifted to 37ºC for additional 3h. During infection and later incubation the respective compounds were present in the media. Cells were stained against NP and analyzed by confocal micoscropy. Mean nuclear intensity was quantified using Image J software. Mann-Whitney test was used for statistical comparison. Shown is one of three independent experiments. Error bars indicate standard deviation of 100 quantified nuclei. **B** Cell viability. Cytotoxic effects of Cbz-Pro treatment were assessed in A549 cells following incubation for 5h. **C** Effect of Cbz-Pro on nuclear NP levels in the presence of cycloheximide. Experimental set-up as in (A). MOI=50 was used for infection and 100 ug/ml cycloheximide-containing medium was added after infection. **D** Sequential treatment with Cbz-Pro and bafilomycin A1 inhibits nuclear NP expression. A549 cells were pre-incubated with 10mM Cbz-Pro or 0.5% MetOH for 2h before infection on ice with A/WSN/33 MOI=10 in the presence of the inhibitor or solvent. After infection, cells were shifted to 37°C for 3h. 1h post-infection, Cbz-Pro or MetOH was present in the media. Following 30 min of incubation with both, Cbz-Pro and bafilomycin A1 (10nM) or MetOH, cells were further incubated with bafilomycin A1 or MetOH-containing medium for additional 90 min. Nuclear NP was measured and quantified as described above. Shown is one out of three independent

678 experiments with error bars indicating standard deviation of 100 analyzed nuclei.
679 **E** Extracellular PEPD cannot rescue IAV infection in siPEPD-treated cells. A549
680 cells were transfected with siScr or siPEPD_1. 48h post-transfection, cells were
681 treated with 50nM of recombinant PEPD 1h before, 1h after or during infection
682 with A/WSN/33 MOI=10. Following addition, PEPD was present in the media until
683 3h after infection. Nuclear NP was measured and analyzed as described above.
684 Shown is one out of three independent experiments with error bars indicating
685 standard deviation of 100 quantified nuclei.

686

References

1. **Palese, P., and M. L. Shaw.** 2007. Orthomyxoviridae: The viruses and their replication. *In* D. M. Knipe and P. M. Howley (ed.), Fields Virology, 5th ed, vol. 2. Lippincott Williams and Wilkins, Philadelphia.
2. **Wise, H. M., E. C. Hutchinson, B. W. Jagger, A. D. Stuart, Z. H. Kang, N. Robb, L. M. Schwartzman, J. C. Kash, E. Fodor, A. E. Firth, J. R. Gog, J. K. Taubenberger, and P. Digard.** 2012. Identification of a novel splice variant form of the influenza A virus M2 ion channel with an antigenically distinct ectodomain. PLoS pathogens **8:**e1002998.
3. **Baum, L. G., and J. C. Paulson.** 1990. Sialyloligosaccharides of the respiratory epithelium in the selection of human influenza virus receptor specificity. Acta Histochem Suppl **40:**35-38.
4. **Edinger, T. O., M. O. Pohl, and S. Stertz.** 2014. Entry of influenza A virus: host factors and antiviral targets. J Gen Virol **95:**263-277.
5. **Patterson, S., J. S. Oxford, and R. R. Dourmashkin.** 1979. Studies on the mechanism of influenza virus entry into cells. J Gen Virol **43:**223-229.
6. **Matlin, K. S., H. Reggio, A. Helenius, and K. Simons.** 1981. Infectious entry pathway of influenza virus in a canine kidney cell line. The Journal of cell biology **91:**601-613.
7. **Yoshimura, A., K. Kuroda, K. Kawasaki, S. Yamashina, T. Maeda, and S. Ohnishi.** 1982. Infectious cell entry mechanism of influenza virus. Journal of virology **43:**284-293.
8. **de Vries, E., D. M. Tscherne, M. J. Wienholts, V. Cobos-Jimenez, F. Scholte, A. Garcia-Sastre, P. J. Rottier, and C. A. de Haan.** 2011. Dissection of the influenza A virus endocytic routes reveals macropinocytosis as an alternative entry pathway. PLoS pathogens **7:**e1001329.
9. **Sieczkarski, S. B., and G. R. Whittaker.** 2002. Influenza virus can enter and infect cells in the absence of clathrin-mediated endocytosis. Journal of virology **76:**10455-10464.
10. **Maeda, T., and S. Ohnishi.** 1980. Activation of influenza virus by acidic media causes hemolysis and fusion of erythrocytes. FEBS Lett **122:**283-287.
11. **Daniels, R. S., J. C. Downie, A. J. Hay, M. Knossow, J. J. Skehel, M. L. Wang, and D. C. Wiley.** 1985. Fusion mutants of the influenza virus hemagglutinin glycoprotein. Cell **40:**431-439.
12. **White, J. M., and I. A. Wilson.** 1987. Anti-peptide antibodies detect steps in a protein conformational change: low-pH activation of the influenza virus hemagglutinin. The Journal of cell biology **105:**2887-2896.
13. **Wharton, S. A., R. B. Belshe, J. J. Skehel, and A. J. Hay.** 1994. Role of virion M2 protein in influenza virus uncoating: specific reduction in the rate of membrane fusion between virus and liposomes by amantadine. J Gen Virol **75 (Pt 4):**945-948.

14. **Zhirnov, O. P.** 1990. Solubilization of matrix protein M1/M from virions occurs at different pH for orthomyxo- and paramyxoviruses. Virology **176:**274-279.
15. **O'Neill, R., R. Jaskunas, G. Blobel, P. Palese, and J. Moroianu.** 1995. Nuclear import of influenza virus RNA can be mediated by viral nucleoprotein and transport factors requiered for protein import. J.Biol.Chem. **270:**22701-22704.
16. **Davies, W. L., R. R. Grunert, R. F. Haff, J. W. McGahen, E. M. Neumayer, M. Paulshock, J. C. Watts, T. R. Wood, E. C. Hermann, and C. E. Hoffmann.** 1964. Antiviral Activity of 1-Adamantanamine (Amantadine). Science **144:**862-863.
17. **Skehel, J. J., A. J. Hay, and J. A. Armstrong.** 1978. On the mechanism of inhibition of influenza virus replication by amantadine hydrochloride. J Gen Virol **38:**97-110.
18. **Hay, A. J., A. J. Wolstenholme, J. J. Skehel, and M. H. Smith.** 1985. The molecular basis of the specific anti-influenza action of amantadine. Embo J **4:**3021-3024.
19. **Kim, C. U., W. Lew, M. A. Williams, H. Liu, L. Zhang, S. Swaminathan, N. Bischofberger, M. S. Chen, D. B. Mendel, C. Y. Tai, W. G. Laver, and R. C. Stevens.** 1997. Influenza neuraminidase inhibitors possessing a novel hydrophobic interaction in the enzyme active site: design, synthesis, and structural analysis of carbocyclic sialic acid analogues with potent anti-influenza activity. Journal of the American Chemical Society **119:**681-690.
20. **Vonitzstein, M., W. Y. Wu, G. B. Kok, M. S. Pegg, J. C. Dyason, B. Jin, T. V. Phan, M. L. Smythe, H. F. White, S. W. Oliver, P. M. Colman, J. N. Varghese, D. M. Ryan, J. M. Woods, R. C. Bethell, V. J. Hotham, J. M. Cameron, and C. R. Penn.** 1993. Rational Design of Potent Sialidase-Based Inhibitors of Influenza Virus Replication. Nature **363:**418-423.
21. **Bright, R. A., M. J. Medina, X. Xu, G. Perez-Oronoz, T. R. Wallis, X. M. Davis, L. Povinelli, N. J. Cox, and A. I. Klimov.** 2005. Incidence of adamantane resistance among influenza A (H3N2) viruses isolated worldwide from 1994 to 2005: a cause for concern. Lancet **366:**1175-1181.
22. **Ison, M. G.** 2011. Antivirals and resistance: influenza virus. Current opinion in virology **1:**563-573.
23. **Hao, L., A. Sakurai, T. Watanabe, E. Sorensen, C. A. Nidom, M. A. Newton, P. Ahlquist, and Y. Kawaoka.** 2008. Drosophila RNAi screen identifies host genes important for influenza virus replication. Nature **454:**890-893.
24. **Brass, A. L., I. C. Huang, Y. Benita, S. P. John, M. N. Krishnan, E. M. Feeley, B. J. Ryan, J. L. Weyer, L. van der Weyden, E. Fikrig, D. J. Adams, R. J. Xavier, M. Farzan, and S. J. Elledge.** 2009. The IFITM proteins mediate cellular resistance to influenza A H1N1 virus, West Nile virus, and dengue virus. Cell **139:**1243-1254.

25. **Shapira, S. D., I. Gat-Viks, B. O. Shum, A. Dricot, M. M. de Grace, L. Wu, P. B. Gupta, T. Hao, S. J. Silver, D. E. Root, D. E. Hill, A. Regev, and N. Hacohen.** 2009. A physical and regulatory map of host-influenza interactions reveals pathways in H1N1 infection. Cell **139:**1255-1267.
26. **Karlas, A., N. Machuy, Y. Shin, K. P. Pleissner, A. Artarini, D. Heuer, D. Becker, H. Khalil, L. A. Ogilvie, S. Hess, A. P. Maurer, E. Muller, T. Wolff, T. Rudel, and T. F. Meyer.** 2010. Genome-wide RNAi screen identifies human host factors crucial for influenza virus replication. Nature **463:**818-822.
27. **Watanabe, T., S. Watanabe, and Y. Kawaoka.** 2010. Cellular networks involved in the influenza virus life cycle. Cell host & microbe **7:**427-439.
28. **Konig, R., S. Stertz, Y. Zhou, A. Inoue, H. H. Hoffmann, S. Bhattacharyya, J. G. Alamares, D. M. Tscherne, M. B. Ortigoza, Y. Liang, Q. Gao, S. E. Andrews, S. Bandyopadhyay, P. De Jesus, B. P. Tu, L. Pache, C. Shih, A. Orth, G. Bonamy, L. Miraglia, T. Ideker, A. Garcia-Sastre, J. A. Young, P. Palese, M. L. Shaw, and S. K. Chanda.** 2010. Human host factors required for influenza virus replication. Nature **463:**813-817.
29. **Su, W. C., Y. C. Chen, C. H. Tseng, P. W. Hsu, K. F. Tung, K. S. Jeng, and M. M. Lai.** 2013. Pooled RNAi screen identifies ubiquitin ligase Itch as crucial for influenza A virus release from the endosome during virus entry. Proc Natl Acad Sci U S A **110:**17516-17521.
30. **Ward, S. E., H. S. Kim, K. Komurov, S. Mendiratta, P. L. Tsai, M. Schmolke, N. Satterly, B. Manicassamy, C. V. Forst, M. G. Roth, A. Garcia-Sastre, K. M. Blazewska, C. E. McKenna, B. M. Fontoura, and M. A. White.** 2012. Host modulators of H1N1 cytopathogenicity. PLoS One **7:**e39284.
31. **Stertz, S., and M. L. Shaw.** 2011. Uncovering the global host cell requirements for influenza virus replication via RNAi screening. Microbes Infect **13:**516-525.
32. **Sakai, T., M. Ohuchi, M. Imai, T. Mizuno, K. Kawasaki, K. Kuroda, and S. Yamashina.** 2006. Dual wavelength imaging allows analysis of membrane fusion of influenza virus inside cells. Journal of virology **80:**2013-2018.
33. **Pasqual, G., J. M. Rojek, M. Masin, J. Y. Chatton, and S. Kunz.** 2011. Old world arenaviruses enter the host cell via the multivesicular body and depend on the endosomal sorting complex required for transport. PLoS pathogens **7:**e1002232.
34. **McClure, M. O., M. A. Sommerfelt, M. Marsh, and R. A. Weiss.** 1990. The pH independence of mammalian retrovirus infection. J Gen Virol **71 (Pt 4):**767-773.
35. **Perez, L., and L. Carrasco.** 1994. Involvement of the vacuolar H(+)-ATPase in animal virus entry. J Gen Virol **75 (Pt 10):**2595-2606.
36. **Galloway, C. J., G. E. Dean, M. Marsh, G. Rudnick, and I. Mellman.** 1983. Acidification of macrophage and fibroblast endocytic vesicles in vitro. Proc Natl Acad Sci U S A **80:**3334-3338.

37. **Yang, L., Y. Li, Y. Ding, K. S. Choi, A. L. Kazim, and Y. Zhang.** 2013. Prolidase directly binds and activates epidermal growth factor receptor and stimulates downstream signaling. The Journal of biological chemistry **288:**2365-2375.
38. **Yang, L., Y. Li, and Y. Zhang.** 2014. Identification of prolidase as a high affinity ligand of the ErbB2 receptor and its regulation of ErbB2 signaling and cell growth. Cell death & disease **5:**e1211.
39. **Eierhoff, T., E. R. Hrincius, U. Rescher, S. Ludwig, and C. Ehrhardt.** 2010. The epidermal growth factor receptor (EGFR) promotes uptake of influenza A viruses (IAV) into host cells. PLoS pathogens **6:**e1001099.
40. **Zona, L., J. Lupberger, N. Sidahmed-Adrar, C. Thumann, H. J. Harris, A. Barnes, J. Florentin, R. G. Tawar, F. Xiao, M. Turek, S. C. Durand, F. H. Duong, M. H. Heim, F. L. Cosset, I. Hirsch, D. Samuel, L. Brino, M. B. Zeisel, F. Le Naour, J. A. McKeating, and T. F. Baumert.** 2013. HRas signal transduction promotes hepatitis C virus cell entry by triggering assembly of the host tetraspanin receptor complex. Cell host & microbe **13:**302-313.
41. **Guinea, R., and L. Carrasco.** 1995. Requirement for vacuolar proton-ATPase activity during entry of influenza virus into cells. Journal of virology **69:**2306-2312.
42. **Inglis, S. C., A. R. Carroll, R. A. Lamb, and B. W. Mahy.** 1976. Polypeptides specified by the influenza virus genome I. Evidence for eight distinct gene products specified by fowl plague virus. Virology **74:**489-503.
43. **Huotari, J., N. Meyer-Schaller, M. Hubner, S. Stauffer, N. Katheder, P. Horvath, R. Mancini, A. Helenius, and M. Peter.** 2012. Cullin-3 regulates late endosome maturation. Proc Natl Acad Sci U S A **109:**823-828.
44. **Lupi, A., A. Rossi, P. Vaghi, A. Gallanti, G. Cetta, and A. Forlino.** 2005. N-benzyloxycarbonyl-L-proline: an in vitro and in vivo inhibitor of prolidase. Biochimica et biophysica acta **1744:**157-163.
45. **Surazynski, A., W. Miltyk, I. Prokop, and J. Palka.** 2010. Prolidase-dependent regulation of TGF beta (corrected) and TGF beta receptor expressions in human skin fibroblasts. European journal of pharmacology **649:**115-119.
46. **Mock, W. L., and P. C. Green.** 1990. Mechanism and inhibition of prolidase. The Journal of biological chemistry **265:**19606-19610.
47. **Lowther, W. T., and B. W. Matthews.** 2002. Metalloaminopeptidases: common functional themes in disparate structural surroundings. Chemical reviews **102:**4581-4608.
48. **Surazynski, A., W. Miltyk, J. Palka, and J. M. Phang.** 2008. Prolidase-dependent regulation of collagen biosynthesis. Amino acids **35:**731-738.
49. **Kitchener, R. L., and A. M. Grunden.** 2012. Prolidase function in proline metabolism and its medical and biotechnological applications. Journal of applied microbiology **113:**233-247.
50. **Powell, G. F., M. A. Rasco, and R. M. Maniscalco.** 1974. A prolidase deficiency in man with iminopeptiduria. Metabolism: clinical and experimental **23:**505-513.

51. **Freij, B. J., H. L. Levy, G. Dudin, D. Mutasim, M. Deeb, and V. M. Der Kaloustian.** 1984. Clinical and biochemical characteristics of prolidase deficiency in siblings. American journal of medical genetics **19:**561-571.
52. **Isemura, M., T. Hanyu, F. Gejyo, R. Nakazawa, R. Igarashi, S. Matsuo, K. Ikeda, and Y. Sato.** 1979. Prolidase deficiency with imidodipeptiduria. A familial case with and without clinical symptoms. Clinica chimica acta; international journal of clinical chemistry **93:**401-407.
53. **Surazynski, A., S. P. Donald, S. K. Cooper, M. A. Whiteside, K. Salnikow, Y. Liu, and J. M. Phang.** 2008. Extracellular matrix and HIF-1 signaling: the role of prolidase. International journal of cancer. Journal international du cancer **122:**1435-1440.
54. **Palka, J. A., and J. M. Phang.** 1997. Prolidase activity in fibroblasts is regulated by interaction of extracellular matrix with cell surface integrin receptors. Journal of cellular biochemistry **67:**166-175.
55. **Sato, M., M. K. Sardana, W. A. Grasser, V. M. Garsky, J. M. Murray, and R. J. Gould.** 1990. Echistatin is a potent inhibitor of bone resorption in culture. The Journal of cell biology **111:**1713-1723.
56. **Surazynski, A., P. Sienkiewicz, S. Wolczynski, and J. Palka.** 2005. Differential effects of echistatin and thrombin on collagen production and prolidase activity in human dermal fibroblasts and their possible implication in beta1-integrin-mediated signaling. Pharmacological research : the official journal of the Italian Pharmacological Society **51:**217-221.
57. **Pleschka, S., T. Wolff, C. Ehrhardt, G. Hobom, O. Planz, U. R. Rapp, and S. Ludwig.** 2001. Influenza virus propagation is impaired by inhibition of the Raf/MEK/ERK signalling cascade. Nat Cell Biol **3:**301-305.
58. **Ehrhardt, C., T. Wolff, S. Pleschka, O. Planz, W. Beermann, J. G. Bode, M. Schmolke, and S. Ludwig.** 2007. Influenza A virus NS1 protein activates the PI3K/Akt pathway to mediate antiapoptotic signaling responses. Journal of virology **81:**3058-3067.

E

007/99

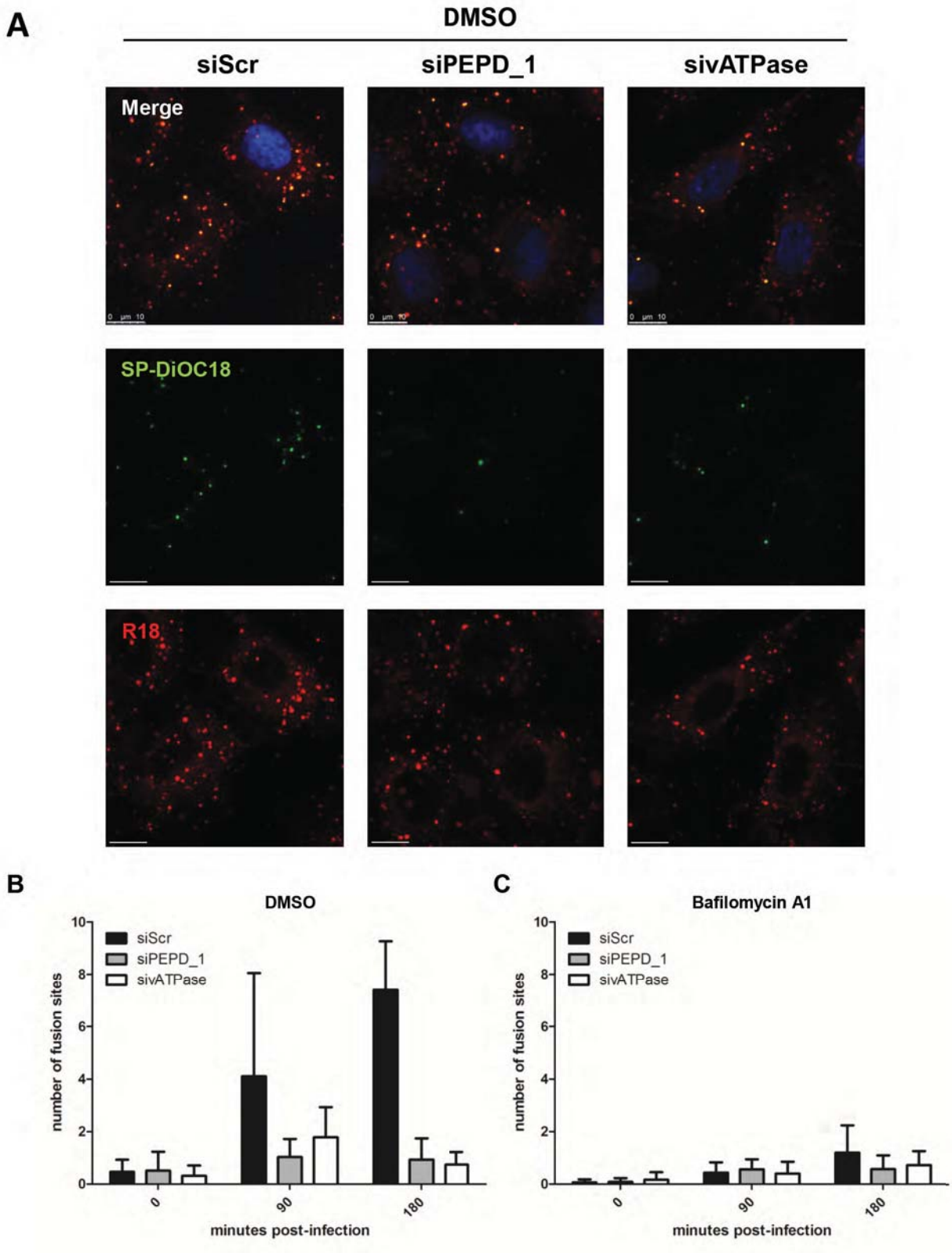
A
DMSO
siScr
siPEPD_1
sivATPase
Merge
SP-DiOC18
R18
B
DMSO
siScr
siPEPD_1
sivATPase
number of fusion sites
minutes post-infection
C
Bafilomycin A1
siScr
siPEPD_1
sivATPase
number of fusion sites
minutes post-infection

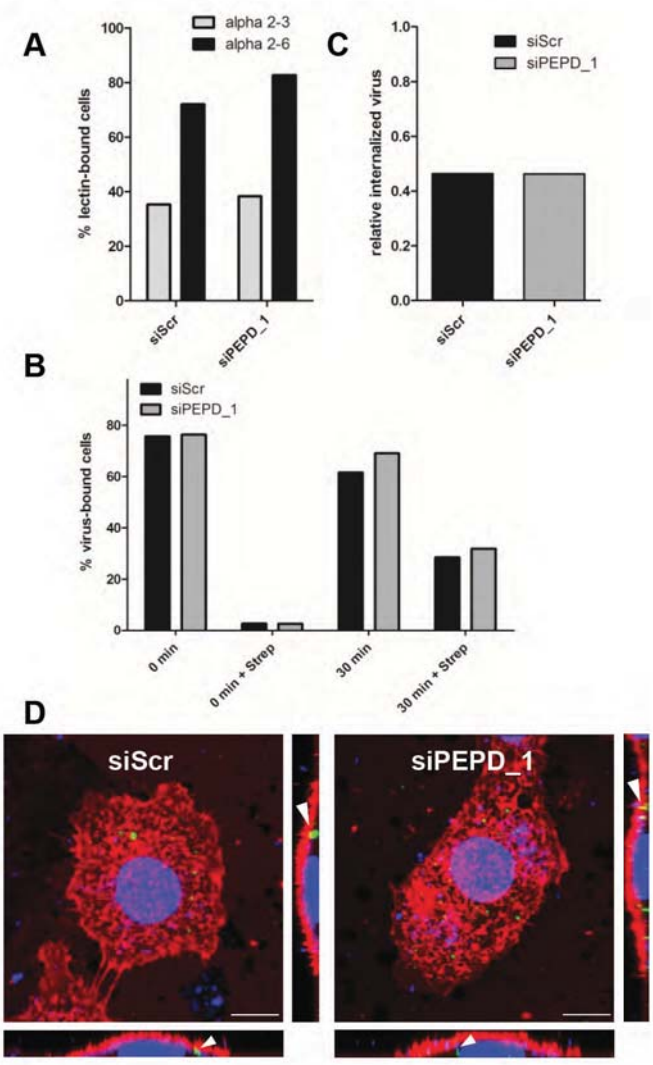
A
alpha 2-3
alpha 2-6
% lectin-bound cells
100
80
60
40
20
0
siScr
siPEPD_1
C
siScr
siPEPD_1
relative internalized virus
1.0
0.8
0.6
0.4
0.2
0.0
siScr
siPEPD_1
B
siScr
siPEPD_1
% virus-bound cells
80
60
40
20
0
0 min
0 min + Strep
30 min
30 min + Strep
D
siScr
siPEPD_1

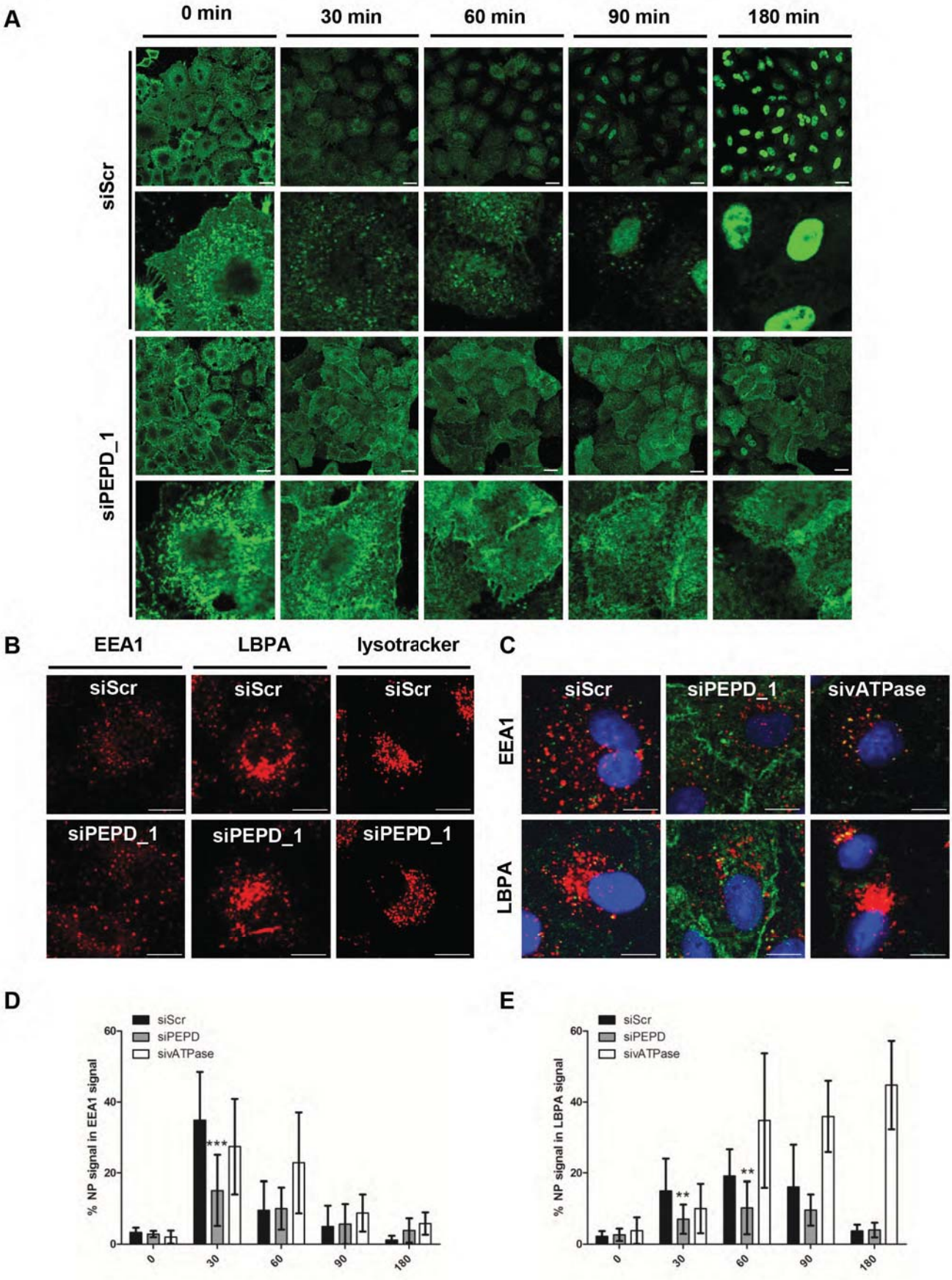
A
0 min
30 min
60 min
90 min
180 min
siScr
siPEPD_1
B
EEA1
LBPA
lysotracker
siScr
siPEPD_1
C
siScr
siPEPD_1
sivATPase
EEA1
LBPA
D
siScr
siPEPD
sivATPase
% NP signal in EEA1 signal
***
E
siScr
siPEPD
sivATPase
% NP signal in LBPA signal
**
**

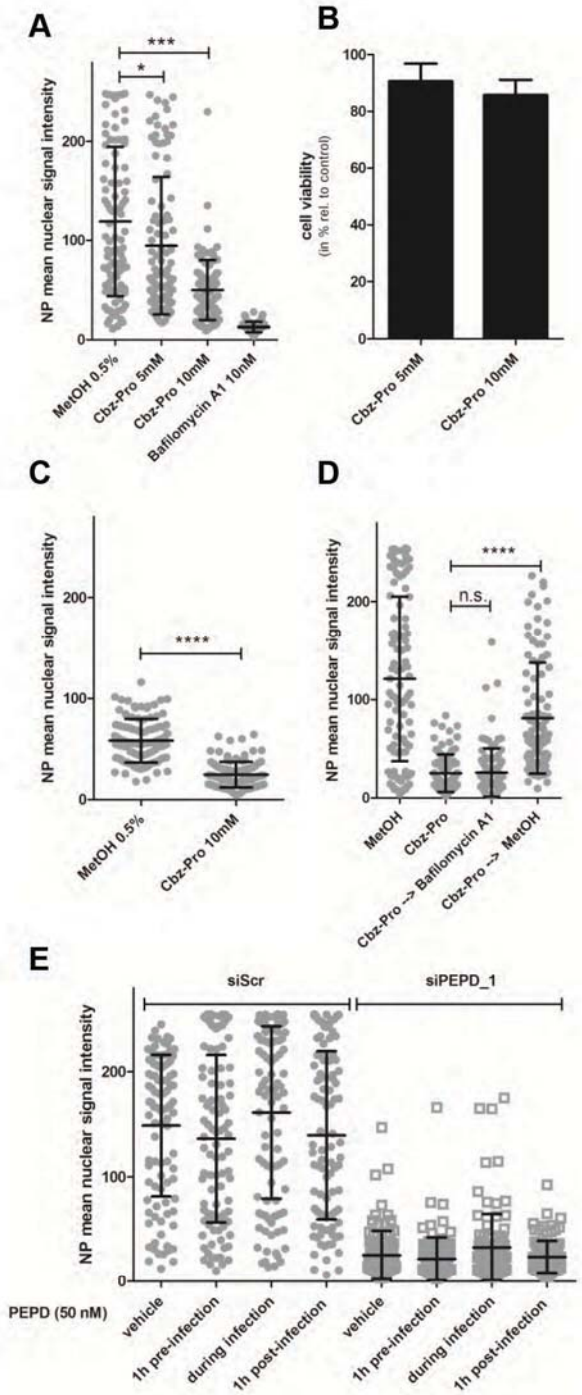
A
B
C
D
E
NP mean nuclear signal intensity
cell viability
(in % rel. to control)
MetOH 0.5%
Cbz-Pro 5mM
Cbz-Pro 10mM
Bafilomycin A1 10nM
MetOH
Cbz-Pro
Cbz-Pro --> Bafilomycin A1
Cbz-Pro --> MetOH
n.s.
siScr
siPEPD_1
PEPD (50 nM)
vehicle
1h pre-infection
during infection
1h post-infection